

# Impairment analysis of WDM Ro-FSO system under different weather conditions employing machine learning

SANMUKH KAUR\*, AANCHAL SHARMA

*Amity School of Engineering & Technology, Amity University Uttar Pradesh, Noida, 201313, India*

In this work, a WDM Ro-FSO communication system has been designed for transmitting data at 80 Gbps with 8 different channels carrying phase shift keying (PSK) modulated signals over a wavelength range of 1546.91 nm to 1552.52 nm at a data rate of 10 Gbps. Quality of signal received at the output of each channel has been analysed for clear air, low haze, heavy haze, and light fog conditions. Artificial neural network (ANN) and support vector machine (SVM) techniques have been implemented to investigate and predict the signal impairments at the receiving end. Root mean square error (RMSE) and  $R^2$  values of 0.148 and 0.98 respectively have been observed in case of ANN model. With RMSE and  $R^2$  values of 0.937 and 0.76, Linear SVM exhibits the best performance in estimation of Q factor of the received signal.

(Received February 19, 2023; accepted October 6, 2023)

*Keywords:* Ro-FSO, Free space optical communication, Phase shift keying, Fog weather conditions, Machine learning, ANN, SVM

## 1. Introduction

Capacity requirements in optical networks had increased dramatically with the development of 5G technology along with rise in demands of applications related to high-definition video and internet of things. To fulfil these demands, low-margin networks employing optical fiber and free space optics (FSO) are attracting attentions [1, 2]. Planning tools with higher accuracy and accurate models for prediction of impairments and quality of transmission (QoT) are the key elements to achieve this. As modern optical networks are heterogeneous in nature, it is difficult to build accurate modelling and monitoring tools employing traditional analytical methods. Data-driven artificial intelligence (AI) and machine learning (ML) provides a promising path for predicting the signal impairments and enabling optical performance monitoring (OPM) [3, 4].

FSO a.k.a. “Optical Wireless” or “Fibreless Optics” is a wireless communication technology that relies on an optical light source to transmit information from one location to another. FSO communication employs same principles and have similar capabilities as with an optical fiber at a reduced cost. Optical light transitions take place above the atmosphere rather than in the fiber's core in order to eliminate both optical fiber costs and elapsed time. Numerous other benefits of this technology include higher data rate transmission, low power consumption, high security, immunity to radio frequency interference and high bandwidth [5, 6].

FSO technology can support the rapid growth of bandwidth requirements arising from different cloud applications including internet and cell phones. The technology being wireless, can create more flexible networks than optical fibers leading to decrease in power consumption and faster deployment [7].

A drawback of the FSO communication is that the line of sight (LOS) propagation is required for accurately

conveying the optical signals from the transmitter to receiver. The sensitivity to atmospheric medium, where fog remains as the main source of attenuation results in amplitude and the phase changes of the received signal.

The light transmission through the atmosphere is significantly impacted by different weather conditions such fog, rain, haze, snow, and smoke [8]. Atmosphere's medium also experiences random variations in air temperature (turbulence), where the turbulence is caused by eddies or distinct cells that function as refraction indices. Scintillation results from changes in the phase and amplitude of the optical beam as a result of interaction with the turbulent medium [9].

The optical beam of light must travel through air medium with extreme accuracy in order to minimize the deterioration of the signal received at the other end of radio over free space optics (Ro-FSO) communications system. Relationship between the optical wavelength size and atmospheric particle size determines that the longer wavelength of a laser source perform well than the shorter ones in the given range of allowed wavelength spectrum. For example, 1550 nm is preferred choice as compared to 1310 nm or 750 nm [10].

Over the past few years, Ro-FSO system have attained significant stature and is being considered as one of the effective data transmission technologies for 5G applications and for delivering high-speed broadband communication links in rural areas [11].

A digital radio signal operating in the frequency range of 3 kHz to 300 GHz is used in radio frequency (RF), wireless communication system for sending data over the air [12, 13]. The first transmission of RF signals modulated over free space optics employed transmitter and receiver and two optical fibers to control the signal through an FSO connection [14]. In 2014, two modes division multiplexing (MDM) channels, (LG00) and (LG10), each carrying data at 20 Gbps over 1 m length, have been created by employing hybrid orthogonal

frequency division multiplexing (OFDM) scheme over Ro-FSO system to transport data at 40 Gbps [15].

Wave division multiplexing (WDM) has also been researched for sending distinct wavelengths through FSO link. In 2015, Ro-FSO communication system have been utilised to load 10 Gbps of data onto four separate WDM channels (2.5 Gbps x 4), each of which carried 2.5 Gbps across a 2 km-long atmospherically attenuated medium [16].

Interest in OPM has increased as a result of advancements in optical networking, particularly with regard to signal quality metrics including optical signal-to-noise ratio (SNR), Q-factor, and dispersion. The sophisticated monitoring techniques may allow fault management and quality-of-service (QoS) monitoring to be expanded into the optical domain [17]. Table 1 depicts the review of different data analysis techniques employed for given performance targets in optical networks.

In this work, we present a WDM Ro-FSO communication model for transmitting data at 80 Gbps.

Different channels occupy bandwidth over a wavelength range from 1514.38 nm to 1547.98 nm and carry signals at data rate of 10 Gbps. Performance of the system has been investigated under clear air, low haze, heavy haze, and light fog conditions and ML techniques have been employed for prediction of signal impairments at the receiving end.

## 2. Proposed system model

Schematic diagram of the proposed WDM Ro-FSO communication system is shown in Fig. 1. Continuous wave (CW) laser wavelengths of 1546.91, 1547.71, 1548.51, 1549.31, 1550.11, 1550.91, 1551.72 and 1552.52 nm have been employed to transport 80 Gbps of information over wireless propagation channel under different weather conditions. Each MZM optically modulates a PSK electrical signal to generate corresponding wavelength channel.

Table 1. Optical performance monitoring employing different modelling targets

Reference No.	Objective	Data Analysis Technique	Performance Target
[17]	Optical performance monitoring and modulation format identification	Principal component analysis	OSNR, CD and DGD monitoring
[18]	Channel estimation in FSO communication system	Deep Neural Network	Symbol Error Rate
[19]	Channel coefficients estimation in FSO link with optical turbulence generating chamber	Maximum likelihood estimation, Bayesian estimation	BER monitoring
[20]	Deep Learning for Improving performance of OOK Modulation over FSO Turbulent Channels	Deep learning, maximum likelihood estimation	SNR, BER monitoring
[21]	Optical performance monitoring from directly detected PDM- QAM signals	Neural Network, Support Vector Machine	OSNR Estimation, modulation format classification
[22]	OSNR Monitoring by Deep Neural Networks trained with Asynchronously sampled data	Deep Neural Network	OSNR monitoring
[23]	Optical performance monitoring of QPSK signals using parameters derived from Balanced- Detected Asynchronous diagrams	Artificial Neural Network	OSNR, CD and DGD monitoring
[24]	Machine- learning method for quality of Transmission Prediction of unestablished Light paths	K-nearest neighbours, Random Forest	BER monitoring

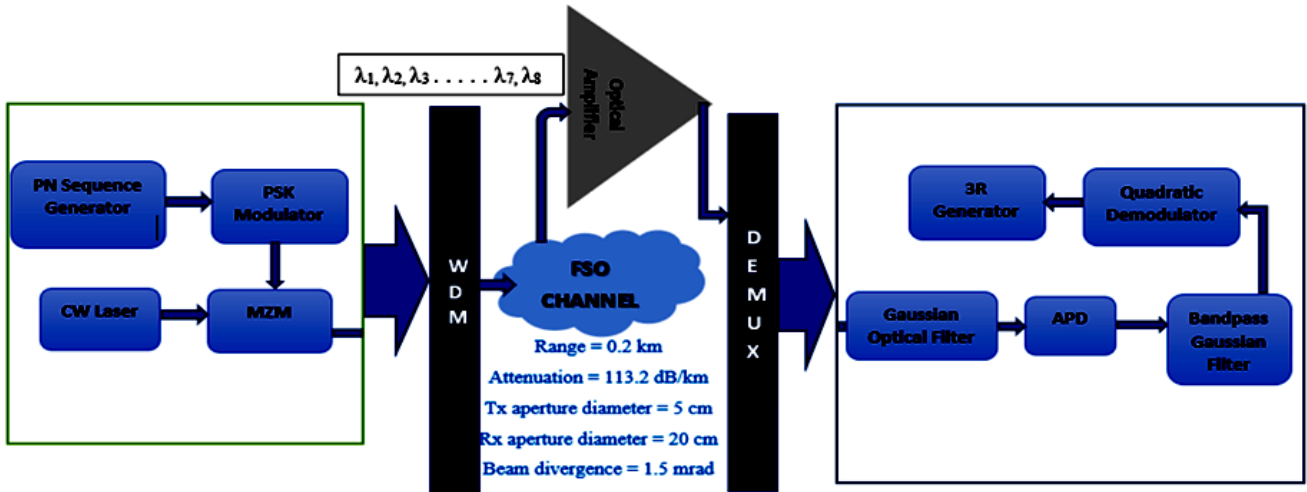


Fig. 1. Block schematic of eight-channel WDM Ro-FSO system (color online)

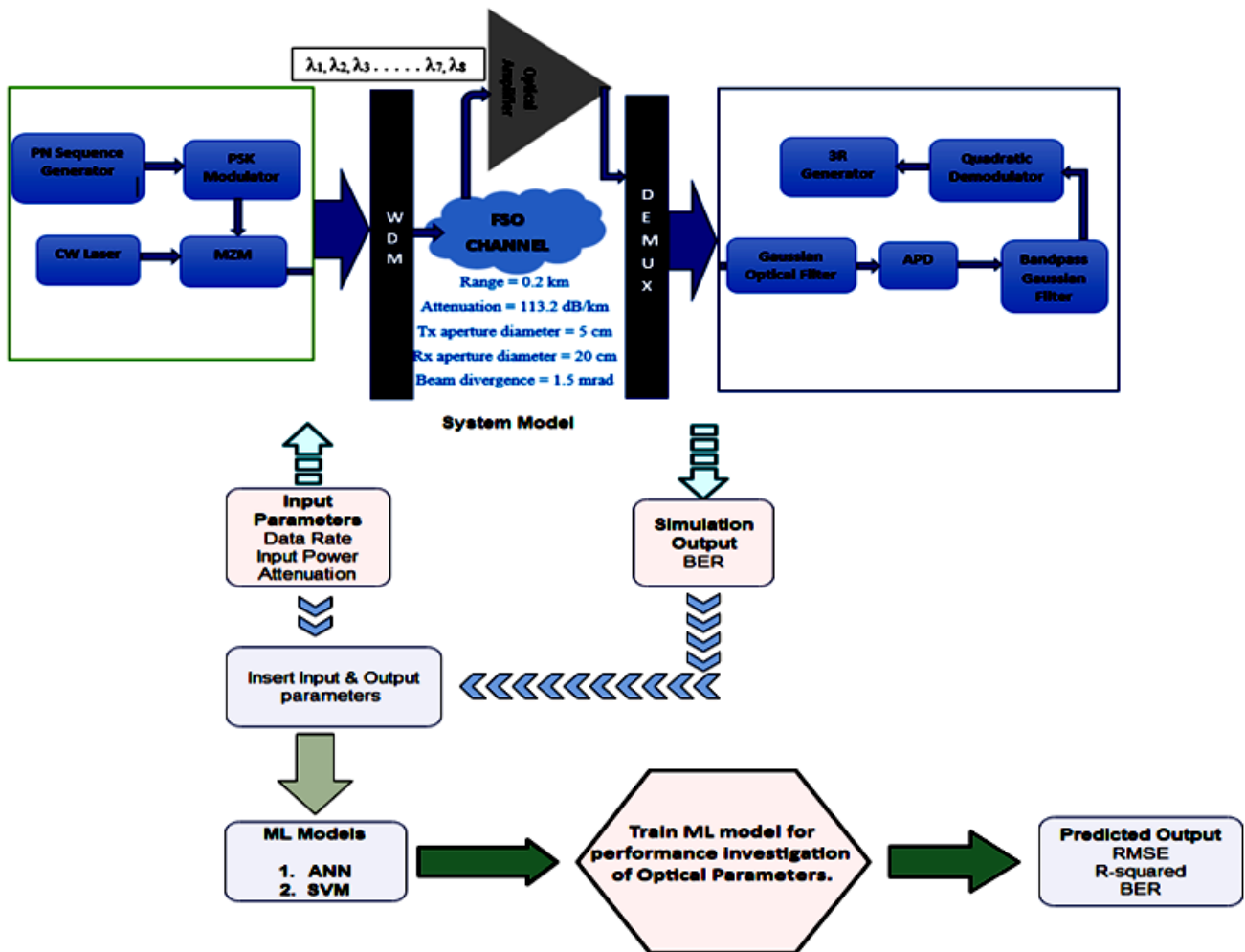


Fig. 2. Block schematic of WDM Ro-FSO system employing ML (color online)

Eight MZMs are employed in the system to generate optical modulated signals, which when combined together resulting in a multiplexed signal propagating through the FSO channel. An optical amplifier, an avalanche photodiode (APD), a bandpass filter (BPF) has been employed to extract the transmitted RF or wavelength. A

quadrature de-modulator extracts the input data from the corresponding channel and delivers at the output. The wavelengths are split and distributed at the receiver as a result of wavelength division de-multiplexing (De-WDM). WDM Ro-FSO system uses phase shift keying (PSK) for generating digitally modulated RF signals. The carrier

wave's phase changes but the amplitude of the electrical modulated PSK signal remains constant. When using methods of (I Q) input signals, the PSK approach might be termed as QPSK. Two parallel sequences are created from the input message as given in equations (1), (2) [25].

$$I_t = s_1 = \sqrt{E} \cos \theta \quad (1)$$

$$Q_t = s_2 = \sqrt{E} \sin \theta \quad (2)$$

$$\theta = \frac{2\pi}{M} (i - 1) + \Phi, \text{ and } M = 2^h \quad (3)$$

where  $M$  is the number of a possible sequence of binary digits,  $h$  is the number of bits per symbol,  $\Phi$  is the phase

$$s_k = \sqrt{2E/T_b} \cos \theta \times \cos(2\pi f_c t) - \sqrt{\frac{2E}{T_b}} \sin \theta \times \sin(2\pi f_c t) \quad (6)$$

This electric RF signal is modulated into an optical wave (a laser) by Mach-Zehnder modulator (MZM) in order to be sent via free space optical link. Received power at the other end of the FSO link is expressed as:

$$P_{received} = P_{transmitted} \frac{d_r^2}{(d_t + \theta L_b)^2} 10^{-0.1\alpha L_b} \quad (7)$$

where  $L_b$  is the path length,  $d_t$  and  $d_r$  represent the transmitter and receiver aperture diameters in meters (m) respectively,  $\theta$  is the beam divergence in milliradians (mrad) and  $\alpha$  is the atmospheric attenuation (dB / km).

Molecular aerosol absorption and scattering causes attenuation of the optical signal which can be expressed in terms of specific attenuation coefficient in dB / Km. Fog particles are formed by fine droplets of water or ice which are spread near the Earth's surface, these are characterized by size, humidity, distribution coefficient and temperature. FSO link operating wavelength may be chosen so that size of the particles is not comparable to the wavelength resulting in lower value of absorption loss. Thus, contribution of scattering is more in the total attenuation.

Different empirical models use visibility data, obtained from the meteorological departments in cities to estimate the fog attenuation. The attenuation coefficient  $\rho_{fog}$  is expressed using Kruse model and is a function of visibility range  $L$  (km) and wavelength of operation,  $\lambda$  ( $\mu\text{m}$ ).

$$\rho_{fog} = \frac{13}{L} \left( \frac{\lambda}{0.55} \right)^{-q}, \quad \text{dB/Km} \quad (8)$$

where  $q$  represents the size distribution of scattering particles and its value is determined as:

$$\begin{aligned} q &= 1.6 \text{ for high visibility } (L > 50 \text{ Km}) \\ &1.3 \text{ for average visibility } (6 \text{ Km} < L < 50 \text{ Km}) \\ &0.585 L^{1/3} \text{ for low visibility } (L > 6 \text{ Km}) \end{aligned} \quad (9)$$

offset. The two signals are applied to modulator multiplier with carrier signals represented by cosine and sign expressions as given in equation (4) and (5) respectively.

$$\Phi_1 = \sqrt{(2/T_b)} \cos(2\pi f_c t) \quad (4)$$

$$\Phi_1 = \sqrt{(2/T_b)} \sin(2\pi f_c t) \quad (5)$$

Here  $f_c$  and  $T_b$  are carrier frequency and bit duration respectively.

Equation (6) represents a phase-variable electrically modulated signal based on the input data conditions where  $\sqrt{E} \cos \theta$  and  $\sqrt{E} \sin \theta$  are the signal's amplitudes.

Specific attenuations (dB / km) considered for the fog and haze weather in the present work have been listed in Table 2.

Table 2. Specific attenuations for various weather conditions [26]

Weather condition	Specific attenuation Value
Clear	0.14 dB / km
Low Haze	1.53 dB / km
Heavy Haze	10.11 dB / km
Light Fog	9 dB / km

Fig. 2 depicts the schematic block diagram of WDM Ro-FSO system employing ML techniques. Data rate, input power and attenuations as a result of different weather conditions have been given as input parameters and features to the simulation and ML model respectively. BER results obtained through simulation has also been applied to ML model as modelling targets. Training the model with ANN and SVM ML algorithms thus predicts the performance in terms of BER for unseen dataset.

### 3. Results and discussion

In order to analyse the proposed WDM based Ro-FSO system, numerical simulations have been carried out employing Optisystem19. Firstly, performance of the system is investigated in terms of quality of received signal under clear air, low haze, heavy haze and light fog conditions. Next artificial neural network (ANN) and support vector machine (SVM) have been utilized to construct predictive models for determination of different performance metrics. Simulation parameters used for analysis of system performance has been listed in Table 3.

Table 3. Simulation parameters

Simulation Parameter	Value
Bit rate	10 Gbps
Transmission power	-5 to 5 dBm
Transmitter aperture diameter	5 cm
Receiver aperture diameter	20 cm
Beam divergence	1.5 mrad
Gain of optical amplifier	10 dB
Optical amplifier Noise figure	3 dB
Gain of APD	10
Responsivity of APD	3 A/W
Dark current of APD	5 nA

Figs. 3 to 6 depict the Q factor of the received signal at the output of the receiver as a function of varying transmission ranges for different atmospheric conditions of clear weather, low haze, heavy haze and light fog respectively. Transmission of information up to 3.3 km, 1.5 km, 0.9 km and 0.4 km have been achieved under clear air, low haze, heavy haze and light fog conditions.

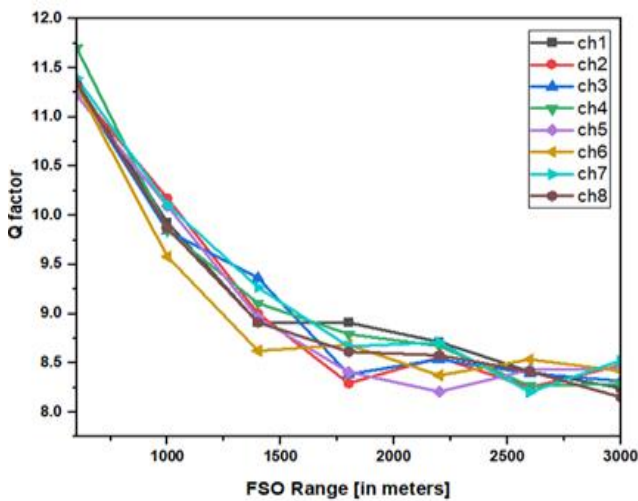


Fig. 3. Q factor versus FSO Range under clear air condition (color online)

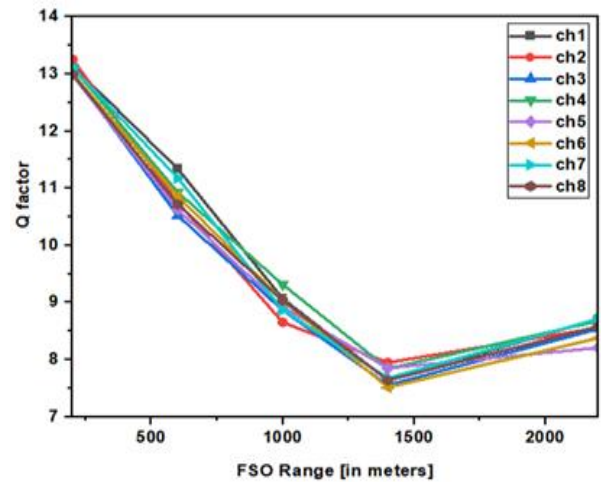


Fig. 4. Q factor versus FSO Range under low haze condition (color online)

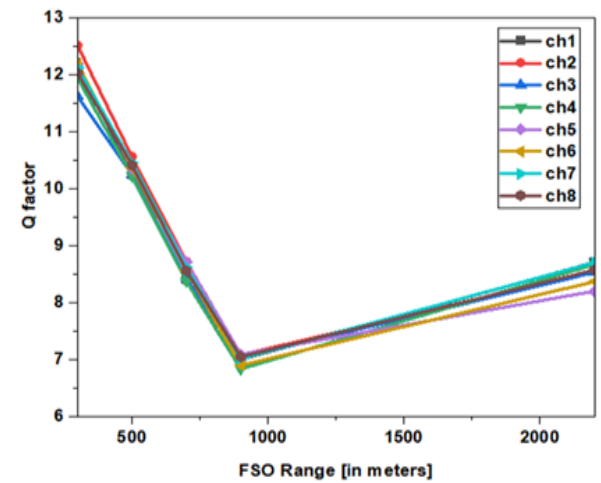


Fig. 5. Q factor versus FSO Range under Heavy haze condition (color online)

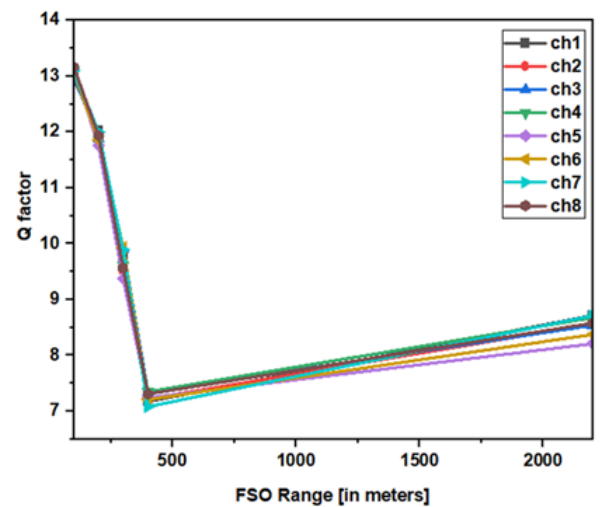


Fig. 6. Q factor versus FSO Range under Light fog condition (color online)

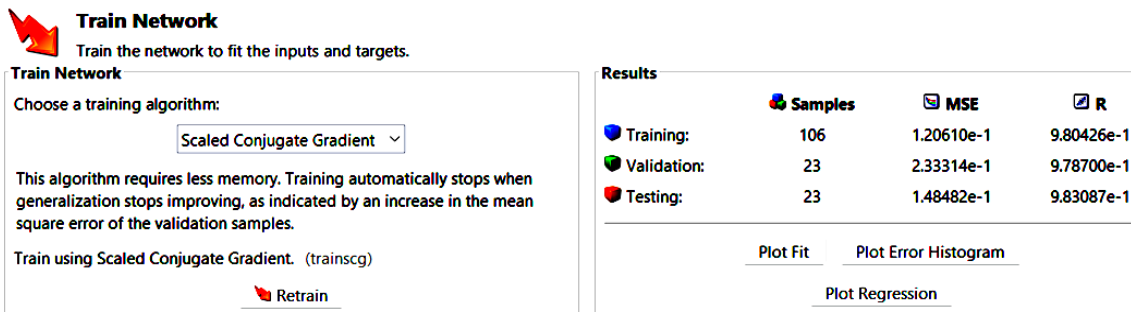


Fig. 7. Scaled conjugate gradient as ANN data training algorithm for Q factor estimation (color online)

Q factor estimation of different channels to investigate the signal impairments at the receiver's end has been carried out at the output of the receiver by employing ANN and SVM as ML techniques. FSO range, attenuations over the turbulent FSO channel, input power level and the number of channels act as some of the input features for the models. Coefficient of determination ( $R^2$ ), root mean square error (RMSE), mean square error (MSE) and mean absolute error (MAE) have been considered as the performance metrics for the analysis.

The scaled conjugate gradient ANN data training algorithm has been employed for analysis based on the input features of FSO range, number of channels, atmospheric attenuation, and input power level. The data has been divided into three subsets of training, validation and testing with percentages of 70%, 15%, and 15%, respectively. The results of ANN model in terms of  $R^2$  values achieved for training, validation and testing data sets along with MSE has been shown in Fig. 7.

RMSE and  $R^2$  values of 0.148 and 0.98 respectively have been observed as shown in the figure. An ANN model with 20 hidden neurons has been trained with number of epochs, performance, gradients and validation

checks to validate the measure of performance (MOP) as shown in Fig. 8.

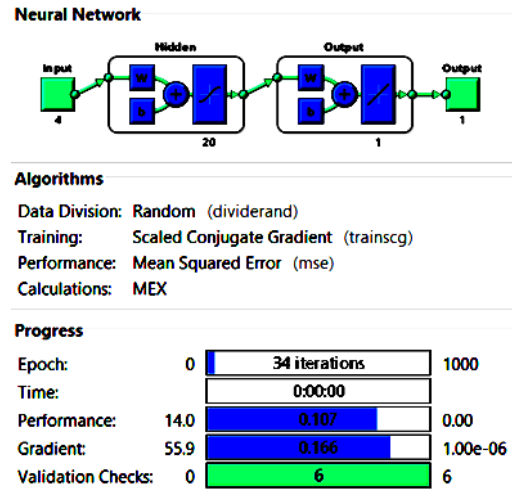


Fig. 8. Neural network with hidden neurons, epochs, performance, gradients and validation checks (color online)

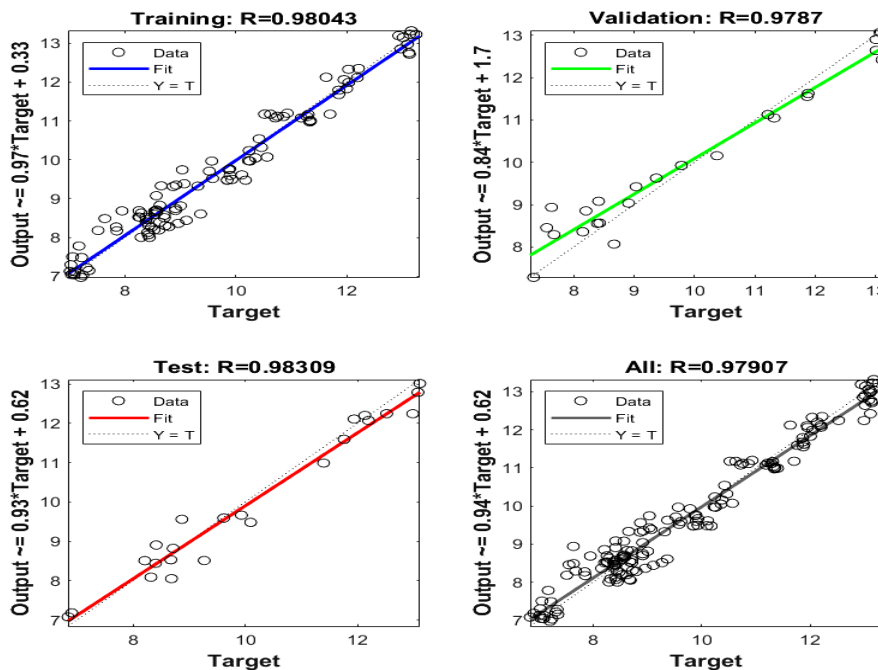


Fig. 9. Regression fit plot for SNR target data set employing ANN (color online)

The results of trained data for the test set with 98.309 percent accuracy and error histogram are shown in Fig. 9 and Fig. 10, respectively.

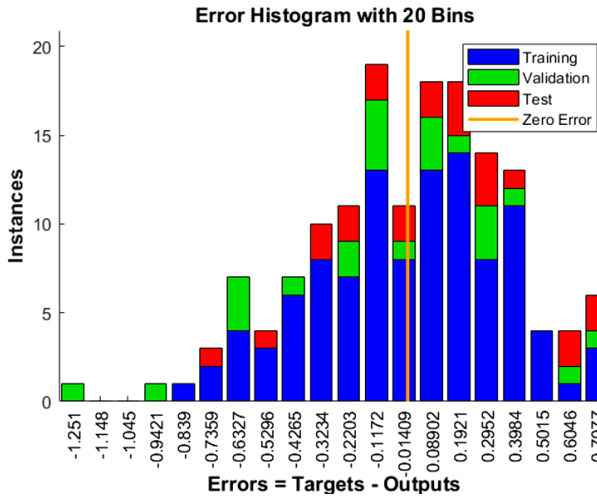


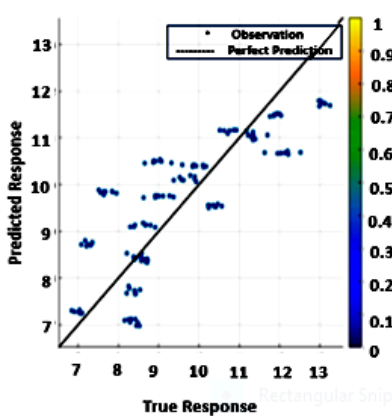
Fig. 10. Error Histogram for SNR target data set employing ANN (color online)

Models		
Sort by:	Model Number	
1.1 SVM	RMSE (Validation): 0.97064	
Last change: Linear SVM 4/4 features		
1.2 SVM	RMSE (Validation): 0.37325	
Last change: Quadratic SVM 4/4 features		
1.3 SVM	RMSE (Validation): <b>0.25693</b>	
Last change: Cubic SVM 4/4 features		
1.4 SVM	RMSE (Validation): 0.78811	
Last change: Fine Gaussian SVM 4/4 features		
1.5 SVM	RMSE (Validation): 0.41011	
Last change: Medium Gaussian SVM 4/4 features		
1.6 SVM	RMSE (Validation): 0.8887	
Last change: Coarse Gaussian SVM 4/4 features		

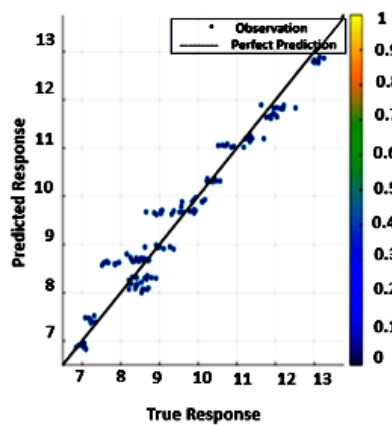
Fig. 11. Regression Models for training data on SVM (color online)

Table 4. Performance comparison of different SVM models

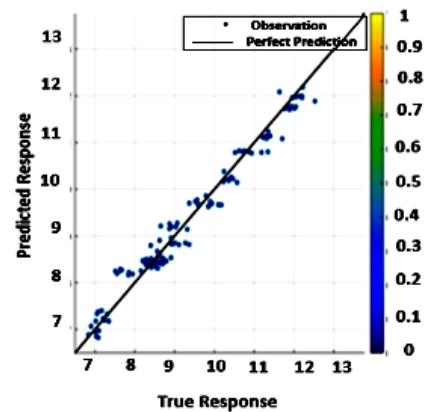
SVM Model	R <sup>2</sup>	RMSE	MSE	MAE
Linear	0.76	0.937	0.879	0.740
Quadratic	0.95	0.415	0.173	0.345
Cubic	0.98	0.271	0.073	0.220
Fine Gaussian	0.70	1.044	1.091	0.870
Medium Gaussian	0.94	0.473	0.224	0.385
Coarse Gaussian	0.69	1.062	1.129	0.838



(a) Linear SVM



(b) Quadratic SVM



(c) Cubic SVM

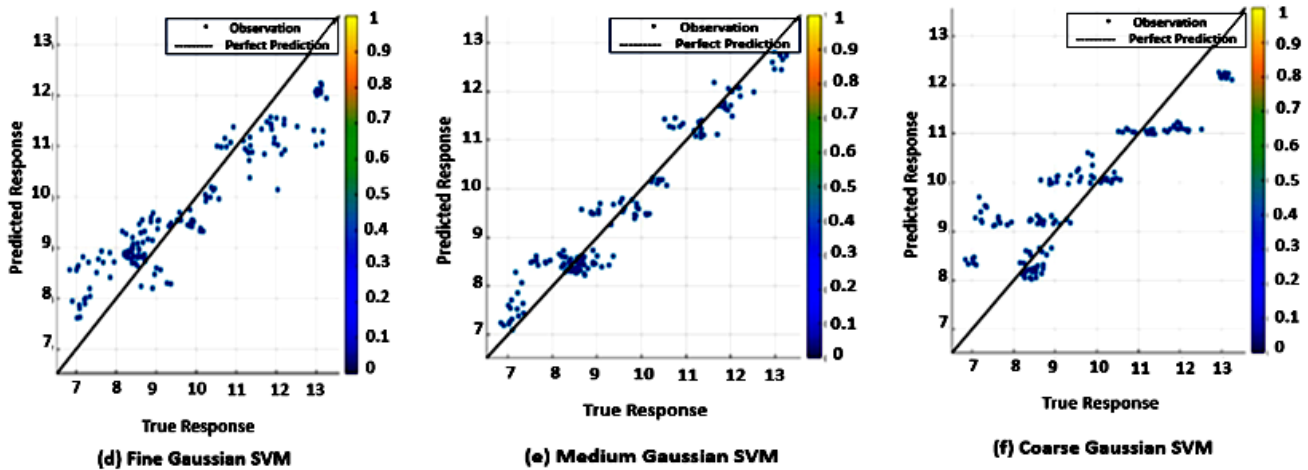


Fig. 12. Response plots of true and predicted values for different SVM Models (color online)

Table 5. Comparative analysis of performance in terms of BER employing SVM model

System Model	Weather Conditions	Attenuation (dB/Km)	Q-Factor	without ML	with ML	Difference
				Log (BER)		
WDM Ro-FSO system	Clear	0.14	13.11	-12.97	-12.86	0.11
	Low Haze	1.53	11.35	-7.57	-7.44	0.13
	Heavy Haze	10.11	6.43	-2.46	-2.21	0.25
	Light Fog	9	7.21	-3.22	-3.00	0.22

Next, Regression Models for training the dataset have been employed to different SVMs i.e., Linear, Quadratic, Cubic, Fine Gaussian, Medium Gaussian and Coarse Gaussian. Performance metrics such as root mean square error (RMSE), coefficient of determination ( $R^2$ ), mean square error (MSE) and mean absolute error (MAE) have been obtained as observed in Fig. 11 and Table 4 respectively. With RMSE and  $R^2$  values of 0.937 and 0.76, Linear SVM exhibits the best performance in estimation of Q factor of the received signal at the receiving end of the proposed Ro-FSO model.

Further, the response plots for true and predicted values of different SVM Models have been depicted in Fig. 12, indicating linear SVM as the best fit model.

Table 5 depicts the comparative analysis of performance of the proposed system in terms of BER obtained through simulation and by employing ML model. It has been observed that the ML model performs well in validating the results and prediction of the performance of the system.

#### 4. Conclusion

WDM Ro-FSO wireless communication system has been used to transmit digital signals at a data rate of 80 Gbps under four different weather conditions of clear air, light rain, heavy rain, and light fog. Different electrical signals have been optically modulated using laser sources operating in the frequency range of 193.1 to 193.8 THz. A 20 GHz, RF signal has been transmitted at a data rate of 10 Gbps using PSK modulation technique. To account for the

channel impairments as a result of different weather conditions, prediction accuracies of ANN and SVM classification and regression models have been determined for proposed Ro-FSO model. ANN approach results in an accurate model with RMSE and  $R^2$  values of 0.148 and 0.98 respectively. RMSE and  $R^2$  values of 0.937 and 0.76 suggest linear SVM to be best-fit model in prediction of quality of received signal. It has been observed that the ML model performs well in validating the results and prediction of the performance of the proposed system.

#### References

- [1] Aanchal Sharma, Sanmukh Kaur, *Optik* **248**, 168135 (2021).
- [2] A. Sharma, S. Kaur, *Opt. Quant. Electron.* **53**, 697 (2021).
- [3] Xiaomin Liu, Huazhi Lun, Mengfan Fu, Yunyun Fan, Lilin Yi, Weisheng Hu, Qunbi Zhuge, *Applied Sciences* **10**(1), 363 (2020).
- [4] J. Thrane, J. Wass, M. Piels, J. C. M. Diniz, R. Jones, D. Zibar, *Journal of Lightwave Technology* **35**(4), 868 (2017).
- [5] Jasleen Kaur, Sanmukh Kaur, Aanchal Sharma, Angela Amphawan, *Frequenz* **77**(1-2), 115 (2023).
- [6] Anuranjana, Kaur, Sanmukh, Goyal, Rakesh, *Journal of Optical Communications*, 000010151520200265 (2021).
- [7] L. Darwesh, N. S. Kopeika, *IEEE Access* **8**, 155275 (2020).
- [8] Sanmukh Kaur, Amayika Kakati, *Journal of Optical*



- Communications **41**(4), 463 (2020).
- [9] Z. Ghassemlooy, W. Popoola, S. Rajbhandari, Optical wireless communications system and channel modelling with MATLAB, International Standard Book Number-13: 978-1-4398-5235-4, 2013.
- [10] H. A. Fadhil, A. Amphawan, H. A. B. Shamsuddin, T. H. Abd, H. M. R. Al-Khafaji, S. A. Aljunid, Nasim Ahmed, *Optik* **124**(19), 3969 (2013).
- [11] M. Balasaraswathi, Mehtab Singh, Jyoteesh Malhotra, Vigneswaran Dhasarathan, *Computers and Electrical Engineering* **87**, 106779 (2020).
- [12] Shilpi Verma, Sanmukh Kaur, *J. Opt. Technol.* **88**(6), 297 (2021).
- [13] D. L. Polla, M. B. Wolfson, 2009 IEEE International Symposium on Radio-Frequency Integration Technology (RFIT), Singapore, 2009, p. 5.
- [14] H. H. Refa, J. J. Sluss Jr., H. H. Refai, *Proceedings of SPIE* **0.5793**, 2005.
- [15] A. Amphawan, S. Chaudhary, V. W. S. Chan, *Journal of the European Optical Society - Rapid Publications* **9**, 14041 (2014).
- [16] S. Chaudhary, A. Amphawn, The 4<sup>th</sup> International Conference on Internet Applications, Protocols, and Services, 2015.
- [17] W. S. Saif, M. A. Esmail, M. Ragheb, T. Alshawi, S. A. Alshebeili, *IEEE Communications Surveys and Tutorials* **22**(4), 2839 (2020).
- [18] M. A. Amirabadi, M. H. Kahaei, S. A. Nezamalhoseini, V. T. Vakili, *Optics Communications* **459**, 124989 (2020).
- [19] P. Mishra, Sonali, A. Dixit, V. K. Jain, 2019 IEEE International Conference on Advanced Networks and Telecommunications Systems (ANTS), 2019, p. 1.
- [20] L. Darwesh, N. S. Kopeika, *IEEE Access* **8**, 155275 (2020).
- [21] J. Thrane, J. Wass, M. Piels, J. C. M. Diniz, R. Jones, D. Zibar, *Journal of Lightwave Technology* **35**(4), 868 (2017).
- [22] T. Tanimura, T. Hoshida, J. C. Rasmussen, M. Suzuki, H. Morikawa, 2016 21st OptoElectronics and Communications Conference (OECC) held jointly with 2016 International Conference on Photonics in Switching (PS), 2016, p. 1.
- [23] Waddah S. Saif, Amr M. Ragheb, Bernd Nebendahl, Tariq Alshawi, Mohamed Marey, Saleh A. Alshebeili, *Photonics* **9**, 299 (2022).
- [24] C. Rottondi, L. Barletta, A. Giusti, M. Tornatore, *Journal of Optical Communications and Networking* **10**(2), A286 (2018).
- [25] Ali Grami, *Introduction to Digital Communications*, 2016, <https://www.sciencedirect.com/topics/engineering/quadrature-phase-shift-keying>
- [26] Mehtab Singh, Jyoteesh Malhotra, Ahmad Atieh, Dhiman Kakati, D. Vigneswaran, *Optical Engineering* **59**(11), 116106-1 (2020).

---

\*Corresponding author: sanmukhkaur@gmail.com